

# A macrokinetic and regulator model for myeloma cell culture based on metabolic balance of pathways

Feng Zhou<sup>a</sup>, Jing-Xiu Bi<sup>b</sup>, An-Ping Zeng<sup>c</sup>, Jing-Qi Yuan<sup>a,\*</sup>

<sup>a</sup> Department of Automation, Shanghai Jiao Tong University, 800 Dongchuan Lu, 200240 Shanghai, PR China

<sup>b</sup> National Key Laboratory of Biochemical Engineering, Institute of Process Engineering, Chinese Academy of Science, 100080 Beijing, PR China

<sup>c</sup> Biochemical Engineering Division, German Research Centre for Biotechnology, Mascheroder Weg 1, 38124 Braunschweig, Germany

Received 10 March 2006; received in revised form 3 August 2006; accepted 5 August 2006

## Abstract

A macrokinetic model is proposed to simulate the growth and metabolism of myeloma cell line in batch and fed-batch cultures. The model describes glycolysis, glutaminolysis, the TCA cycle, respiratory chain, formation of metabolites, as well as cell growth and death. In particular, metabolic shift in the glucose utilization is considered in response to the change of glycolysis rate during the cultivation. A closed loop regulator is introduced to approximate the induction of enzyme pool during lag phase after inoculation. Based on the model, the specific consumption rate of substrate, the specific growth rate, the specific acetyl CoA formation rate as well as the specific oxygen uptake rate are estimated. The specific substrate consumption rate and the specific growth rate are then coupled into a bioreactor model, which delivers the key variables, i.e., cell density, substrate and metabolite concentrations. Batch and fed-batch cultivations were used to validate the model.

© 2006 Elsevier Ltd. All rights reserved.

**Keywords:** Myeloma; Metabolic pathways; Stoichiometric model; Regulator model; Metabolic shift

## 1. Introduction

The metabolic behavior of mammalian cells is mainly affected by nutrient concentrations, pH, growth factors, dissolved oxygen and cell density [1–6]. Kinetic modeling is important for better understanding cell physiology and for process control to further optimize animal cell cultures. A number of unstructured models have been proposed to describe the behavior of mammalian cell cultures [7]. Structured models as well as cybernetic models attempted to explain the cell physiology by taking the intracellular fluxes, the activity and the expression of enzymes into account [8–12]. Models based on metabolic pathways as well as energy and mass balances have been used successfully to describe the growth and metabolism of yeast [13–15]. For mammalian cell culture, the metabolic pathways have been investigated by using stoichiometrically based reaction network and metabolic flux analysis [3,16–19]. In mammalian cells, glycolysis is the main pathway to utilize glucose and to yield ATP [1,2]. The specific uptake

rate of glucose increases with the glucose concentration within a specific range [1]. A metabolic shift may be resulted from variation of the specific glucose uptake rate. Recently, the molecular mechanism of metabolic shift has been studied [20]. Extensive experimental investigations on the metabolic shift for hybridoma cell lines have demonstrated decreasing of lactate formation [21–24].

In this paper, a simplified model for myeloma cell line is proposed based on stoichiometric balance. Glutamine and glucose are considered as the main energy sources and anabolic precursors. The specific glycolysis rate is regarded as the key variable to induce the metabolic shift. The model is composed of two modes. First, a rapid-glycolysis mode describes the rapid-glycolysis and glutaminolysis rates to produce lactate and ammonia. Second, in the low-glycolysis mode, the specific glucose consumption rate and the glycolysis rate are declined and the formation of lactate is terminated. For some cell lines, lactate is even taken as substrate in this mode [25]. Balances of carbon source, lactate, alanine, ATP and NADH have been taken into account in the modeling. The reaction rates in the model include the glycolysis rate of glucose, glutaminolysis rate of glutamine, the specific growth rate, the specific acetyl CoA production rate as well as the specific oxygen uptake rate.

\* Corresponding author. Tel.: +86 21 3420 4055; fax: +86 21 3420 4055.  
E-mail address: jqyuan@sjtu.edu.cn (J.-Q. Yuan).

After coupling the macrokinetic model with a bioreactor model, the relationship between substrate feeding rates and the key state variables, such as cell density, substrates and metabolites concentrations, were estimated. Finally, the model was validated by four sets of experimental data.

## 2. Materials and methods

### 2.1. Cell line and culture conditions

X63-Ag8.653 myeloma cell line (without recombinant protein expression) was used. The base medium used in flask and spinner cultures was RPMI-1640 supplemented with 2 mM glutamine, 80 µg/mL gentamicin and 10% fetal calf serum (FCS) (Invitrogen, UK). For batch culture, the initial concentrations of glucose and glutamine were 10 and 2 mM, respectively. The feeding medium FM1 was composed of 100 mM glucose and 20 mM glutamine with 10× RPMI as base medium. FM2 contained 99.4 mM glucose and 22 mM glutamine with 1× RPMI as base medium.

Cells stored in liquid nitrogen were thawed and then grown in 25 and 75 cm<sup>2</sup> T-flasks consecutively. Then, cells were transferred into 250 mL spinner flask with the initial cell density of  $1.0 \times 10^5$  cells/mL for subsequent suspension cultivation until the mid-exponential growth phase was reached. After that, the preculture was transferred to four 300 mL spinners for further experiments. These experiments had an initial cell density of  $1.5 \times 10^5$  cells/mL. The culture temperature was maintained at 37 °C. The agitation rate was set to 120 rpm, while the concentration of CO<sub>2</sub> was controlled at 5%.

### 2.2. Analytical methods

Viable and dead cell densities were determined by the trypan blue exclusion method using a haemocytometer. Glucose and lactate concentrations were measured with a YSI2700 (Ohio, USA) glucose and L-lactate analyzer. Ammonia concentration was determined using enzyme-based assay kits. Glutamine and other amino acid concentrations were measured by HPLC (KONTRON, Germany) and evaluated with the Software Kroma2000.

### 2.3. Experiment

Exp. 1: batch cultivation for 134 h with an initial volume of 150 mL.

Exp. 2: the duplicated experiment of Exp. 1. Sampling assay was carried out only until 81 h.

Exp. 3: fed-batch experiment. Three times feeding were performed during 134 h cultivation with an initial volume of 120 mL. The first feeding was at 54.5 h by feeding 2.5 mL FCS and 8 mL FM2 until the glucose concentration reached 11 mM. Second feeding was at 73 h by feeding 8 mL FCS. Finally, 10 mL FCS and 9.4 mL FM (4.7 FM1 + 4.7 FM2) were fed after 19.4 mL supernatant was removed at 113 h. Then, the culture was continued for another 21 h.

Exp. 4: fed-batch cultivation with an initial volume of 120 mL. 2.5 mL FCS and 3.5 mL FM2 were first fed at 54.5 h until the glucose concentration reached 5.6 mM. Eight-milliliter FCS and 4 mL FM2 were fed at 73 h as the second feeding. At 113 h, 10 mL FCS and 1.3 mL FM1 were fed as the third feeding, before that, 11.3 mL supernatant was removed. The total cultivation time was 134 h.

## 3. Simplified metabolic pathways and stoichiometry in myeloma cell culture

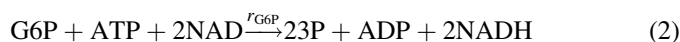
### 3.1. The simplified metabolic pathways

The simplified metabolic pathways of myeloma cell line are schematically shown in Fig. 1. Glucose and glutamine are considered as the main energy sources. The contribution of other amino acids to energy yield is ignored according to

literature [3,26]. Glucose is phosphorylated to glucose 6-phosphate (G6P) by hexokinase at first. Then, G6P is oxidized to 3-phosphoglycerate (3P) by phosphoglucose isomerase, phosphofructo kinase, aldolase, glyceraldehydes 3-phosphate dehydrogenase and phosphoglycerase kinase [2]. Following that, pyruvate is formed from 3P as the outcome of glycolysis via bioreactions catalyzed by phosphoglyceromutase, enolase and pyruvate kinase [2,27]. A part of G6P enters the pentose phosphate pathway (PPP) to produce reducing power (NADPH) and ribose-5-phosphate (R5P), the latter is an important precursor of nucleic acids [28]. Pyruvate either enters the tricarboxylic acid (TCA) cycle via acetyl CoA or is reduced to lactate by consuming NADH [21]. The second major substrate, glutamine, is either deamidated to enter the TCA cycle or directly used for protein synthesis. Glutamate is mainly produced from glutamine metabolism, while the rest is obtained from transamination. α-Ketoglutarate (α-kg) from glutamine utilization is transformed to malate. A part of malate generates oxaloacetate, while the other part, in conjunction with oxaloacetate derived from cytoplasmic acetyl CoA and cysteine and serine, furnishes the cytoplasmic pyruvate pool [29]. In the TCA cycle, citrate is not completely oxidized but mainly leaves the mitochondrion for use in the lipid syntheses [28]. With this supplement of pyruvate, the TCA cycle is balanced [29].

### 3.2. Stoichiometric balance equations

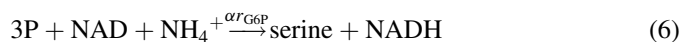
In the following metabolic pathway equations, the unit for all substances is mole. The reactions represented by Eqs. (1)–(23) are corresponded to the pathway number as indicated in Fig. 1. The process of glycolysis is described as follows (pathways 1–3) [2].



where G6P and 3P stand for glucose 6-phosphate and 3-phosphoglycerate, respectively. Simultaneously, a part of G6P is converted to R5P via PPP (pathway 4). R5P is assimilated into cellular constituents (pathway 5) [29]. Where  $r_{\text{Bi}} = \mu K_{\text{Bi}}$ ,  $i = 1, 2, 3, 4$ .



A small part of the 3P is used to synthesize serine and glycine as described by Eqs. (6) and (7) (pathways 6–7) [18].  $\alpha$  is used to describe the fraction of 3P which synthesizes serine.



The metabolic pathways of glutamine metabolism are described as follows (pathways 8–13) [3,18,27,29]. First, the

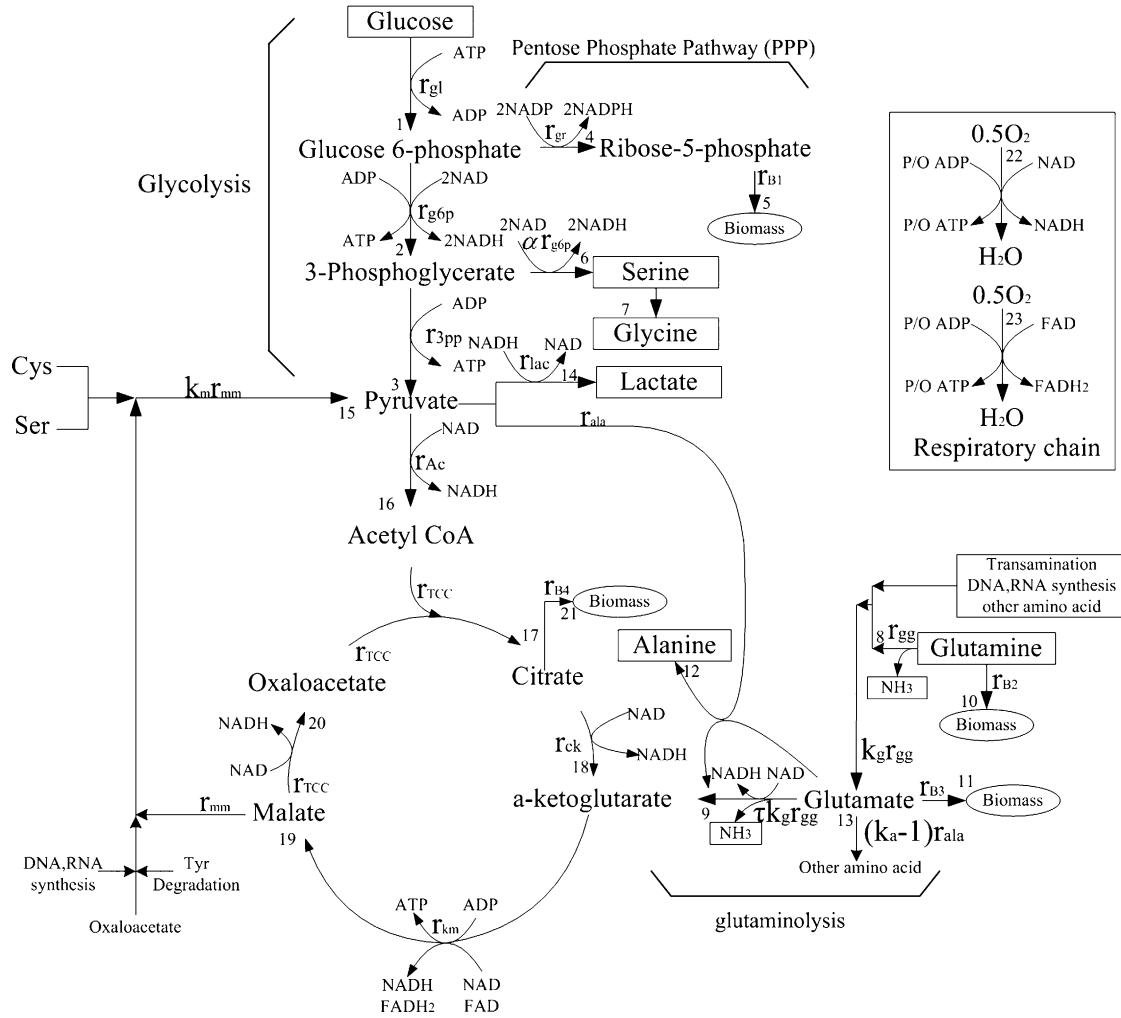
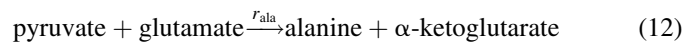
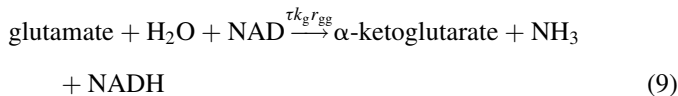
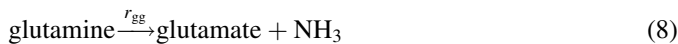
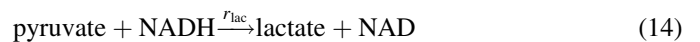


Fig. 1. Simplified metabolic pathways of myeloma cell line (1–23 indicating the number of the pathways to be modeled).

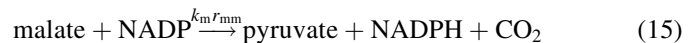
deamidation of glutamine yields glutamate and ammonia, see Eq. (8), where  $r_{gg}$  is the specific production rate of glutamate deaminated from glutamine. Besides glutamine, some other pathways may generate glutamate as well. The total specific production rate of glutamate is denoted by  $k_g r_{gg}$  ( $k_g > 1$ ). A part of the glutamate is converted to  $\alpha$ -kg as described in Eq. (9), which enters the TCA cycle. Another part of glutamate, together with glutamine, is used to prepare protein for biomass formation as indicated by Eqs. (10) and (11). Simultaneously, glutamate reacts with pyruvate to yield alanine and  $\alpha$ -kg, see Eq. (12). Glutamate generates many other amino acids except for alanine. The specific production rate of all these amino acids including alanine is represented by  $k_a r_{ala}$  ( $k_a > 1$ ), see Eq. (13),



Pyruvate is reduced to lactate (pathway 14) [2]:



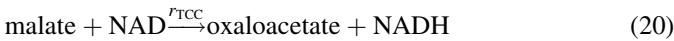
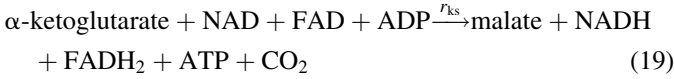
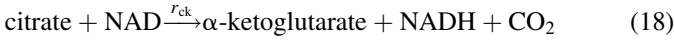
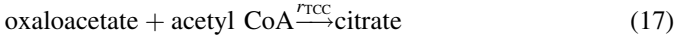
In TCA cycle described below, malate is produced from  $\alpha$ -kg. A part of malate leaves mitochondrion and then supplements the cytoplasmic pyruvate pool. The resulted specific pyruvate production rate is denoted with  $r_{mm}$ . Another part of malate generates oxaloacetate. Some other amino acids in cytoplasm, such as serine and cysteine, also generate pyruvate through malate.  $k_m r_{mm}$  ( $k_m > 1$ ) is used to describe the conversion to pyruvate from malate in cytoplasm (pathway 15) [29]:



The pyruvate is oxidized to acetyl CoA (pathway 16) [3]:



The simplified TCA cycle and the assimilation of acetyl CoA via citrate for cellular constituent formation are presented by Eqs. (17)–(21) (pathways 17–21) [16,29]:



Eqs. (22) and (23) are used to describe the ATP generation in

## 4. Modeling

### 4.1. Model equations for bioreactions' rate

To develop a practically applicable model, a basic assumption is made: the intracellular reactions as given in Eqs. (1)–(24) are assumed to be always in quasi-steady state within each simulation step [13]. This assumption, however, does not mean that the intrinsic dynamic property of the cultivation is overlooked. Instead, the reaction rates will follow immediately the change of external conditions as mediated by the substrate uptake rate or the output of the metabolic regulation. Such assumption has also been applied successfully for yeast and animal cells [31–33]. Then, the macrokinetic model based on the metabolic balance of pathways of intracellular substances and energy are constructed in matrix form, see Eqs. (25) and (26).

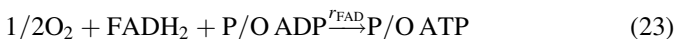
(1)  $r_{3pp} < r_{3pp,min}$ , rapid-glycolysis mode:

$$\begin{bmatrix} 1 & 0 & 0 & K_{B1} & 0 & 0 & 0 \\ 2(1-\alpha) & 0 & 0 & K_{B2} & 0 & 0 & 0 \\ 0 & (1-\tau)k_g & -k_a & -K_{B3} & 0 & 0 & 0 \\ 1 & k_m\tau k_g & k_m - 1 & -k_m K_{B4} & -1 & -1 & 0 \\ \frac{1+2\alpha}{1-\alpha} & 2\tau k_g & 2 & -3K_{B4} & 5 & -1 & -2 \\ 1 & \tau k_g & 1 & -K_{B1} - K_{B4} - \frac{1}{Y_{ATP}} & 1 & 0 & 2P/O \\ 1 & 0 & 0 & 0 & 0 & -\frac{1}{\beta} & 0 \end{bmatrix} \begin{bmatrix} r_{3pp} \\ r_{gg} \\ r_{ala} \\ \mu \\ r_{Ac} \\ r_{lac} \\ r_{O_2} \end{bmatrix} = \begin{bmatrix} r_{glc} \\ r_{gln} \\ 0 \\ 0 \\ 0 \\ m_{ATP} \\ r_{3pp,min} \end{bmatrix} \quad (25)$$

(2)  $r_{3pp} < r_{3pp,min}$ , low-glycolysis mode:

$$\begin{bmatrix} 1 & 0 & 0 & K_{B1} & 0 & 0 \\ 2(1-\alpha) & 0 & 0 & K_{B2} & 0 & 0 \\ 0 & (1-\tau)k_g & -k_a & -K_{B3} & 0 & 0 \\ 1 & k_m\tau k_g & k_m - 1 & -k_m K_{B4} & -1 & 0 \\ \frac{1+2\alpha}{1-\alpha} & 2\tau k_g & 2 & -3K_{B4} & 5 & -2 \\ 1 & \tau k_g & 1 & -K_{B1} - K_{B4} - \frac{1}{Y_{ATP}} & 1 & 2P/O \end{bmatrix} \begin{bmatrix} r_{3pp} \\ r_{gg} \\ r_{ala} \\ \mu \\ r_{Ac} \\ r_{O_2} \end{bmatrix} = \begin{bmatrix} r_{glc} \\ r_{gln} \\ 0 \\ 0 \\ 0 \\ m_{ATP} \end{bmatrix} \quad (26)$$

the respiration chain (pathways 22–23) [28]:



ATP consumption is assumed to be mainly used for cell growth and maintenance [30].

$$r_{ATP} = \frac{\mu}{Y_{ATP}} + m_{ATP} \quad (24)$$

Two different physiological modes are included in the model. Eq. (25) describes the rapid-glycolysis mode, which consists of seven sub-balance models. The first row of Eq. (25) describes the balance of glucose resulted from Eqs. (1) to (5). The second row of Eq. (25) obtained from Eqs. (8) and (9) is the balance for specific glutamine uptake rate. The row 3 stands for the balance of glutamate, which is resulted from Eqs. (8), (10) and (11). Similarly, the row 4 of Eq. (25) stands for the balance of pyruvate, which is resulted from Eqs. (3), (12) and (14)–(16).

The row 5 in Eq. (25) shows the NADH and FADH<sub>2</sub> balance obtained according to Eqs. (2), (6), (9), (14) and (16)–(21).

The derivation of the balance is explained as follow. From Eqs. (2) and (6), the specific production rate of NADH in glycolysis is  $r_{\text{NADH}_G} = ((1 + 2\alpha)/(1 - \alpha))r_{3pp}$ . From Eq. (9), the specific production rate of NADH in glutaminolysis is  $r_{\text{NADH}_G\text{In}} = \tau k_g r_{gg}$ , where  $\tau$  is the fraction of glutamate converted to  $\alpha$ -ketoglutarate. From Eqs. (16), (18)–(20), the specific production rate of NADH in TCA cycle is  $r_{\text{TCC}} + r_{ck} + r_{km} = 3r_{\text{TCC}} - 2r_{B4} + \tau k_g r_{gg} + r_{ala}$ , with  $r_{ck} = r_{\text{TCC}} - r_{B4}$  and  $r_{km} = r_{ck} + \tau k_g r_{gg} + r_{ala}$ , where  $r_{\text{TCC}} = r_{Ac}$ . The specific production rate of  $\text{FADH}_2$  is  $r_{km}$  in TCA cycle. At the same time, pyruvate is converted to lactate accompanied with the consumption of NADH. Finally, the specific turnover rate of NADH and  $\text{FADH}_2$  in the respiratory chain,  $r_{\text{NAD}}$  and  $r_{\text{FAD}}$ , respectively equals  $2r_{O_2}$  as shown in Eq. (22) and (23). Therefore, the balance equation for NADH and  $\text{FADH}_2$  becomes  $((1 + 2\alpha)/(1 - \alpha))r_{3pp} + 2\tau k_g r_{gg} + 5r_{Ac} - 3r_{B4} - r_{lac} - 2r_{O_2} = 0$ .

The row 6 in Eq. (25) is ATP balance obtained from Eqs. (1)–(3) and (17)–(21). During glycolysis, the specific ATP production rate is  $r_{3pp} - r_{B1}$ , see Eqs. (1)–(3). In the TCA cycle, the specific ATP production rate is  $r_{km} = r_{\text{TCC}} - r_{B4} + \tau k_g r_{gg} + r_{ala}$ . In the respiratory chain, the specific ATP production rate is  $2(P/O)r_{O_2}$ , where  $P/O$  is effectiveness coefficient of oxidative phosphorylation. The difference of estimated value of  $P/O$  between NADH and  $\text{FADH}_2$  is neglected in the paper for simplification. According to Eq. (24), the specific ATP consumption rate for cell growth and maintenance is  $\mu/Y_{ATP} + m_{ATP}$ . Therefore, the balance equation for ATP is  $\tau k_g r_{gg} + r_{3pp} + r_{ala} - r_{B1} - r_{B4} - (\mu/Y_{ATP}) + r_{Ac} + 2(P/O)r_{O_2} = m_{ATP}$ .

As described above, the production of lactate from pyruvate is resulted from rapid-glycolysis and the lack of activity of malate–aspartate shuttle to transport NADH into mitochondrion. Therefore, it is assumed that the ability of mitochondrial membrane transporting NADH into mitochondrion has a threshold. When the specific NADH production rate is larger than the threshold, pyruvate is reduced to lactate. Otherwise, the metabolism is shifted to low-glycolysis mode. This hypothesis is described as the row 7 in Eq. (25). The threshold is defined as  $r_{3pp,\text{min}}$ . When  $r_{3pp} \geq r_{3pp,\text{min}}$ , the specific production rate of lactate is  $r_{lac} = \beta(r_{3pp} - r_{3pp,\text{min}})$ , where  $\beta$  is the fraction of pyruvate oxidized to lactate.

Eq. (26) describes the low-glycolysis mode in the case of  $r_{3pp} < r_{3pp,\text{min}}$ , where the generation of lactate ceases. It is obtained by removing the specific production rate of lactate from Eq. (25).

#### 4.2. Model for substrate uptake, the regulator and cell death model

The specific glucose uptake rate is represented as an extended Monod kinetics. The specific glucose uptake rate is influenced by the concentrations of glucose and glutamine and cell density [4,5,34–36].

$$r_{\text{glc},M} = r_{\text{glc},\text{max}} \frac{S_{\text{glc}}}{K_{\text{glc}} + S_{\text{glc}}} \frac{S_{\text{gln}}}{K_{\text{gln}} + S_{\text{gln}}} \frac{k_{\text{cglc}}}{X_v + k_{\text{cglc}}} \quad (27)$$

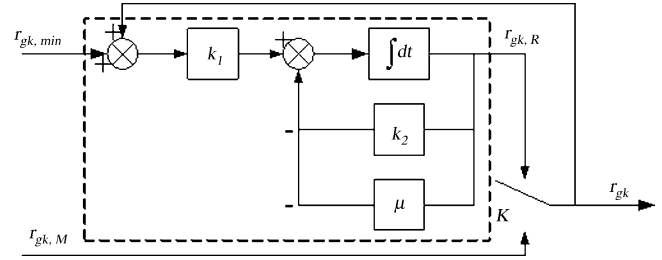


Fig. 2. Diagram of a regulator model for the specific glucose uptake rate.

However, it is found that the real glucose uptake rate is much lower than  $r_{\text{glc},M}$  at the beginning of cultivation, even though the glucose concentration is the highest. Such discrepancy exists for most Monod type models because the Monod model does not take the induction of the enzyme pool involved in glycolysis into account. A regulator model [13,15] is therefore used to deal with such inducing process. Fig. 2 illustrates the structure of the regulator model which consists of basically two control loops, one is the negative feedback loop, and the other is the positive one.  $r_{\text{glc},\text{min}}$  stands for the minimum constitutive activity of the regulated pathway.  $r_{\text{glc},R}$  represents the actual activity of regulated pathway in analogy to enzyme levels of biochemical structure models. At the beginning of cultivation, if  $r_{\text{glc},R} < r_{\text{glc},M}$ , then  $r_{\text{glc}} = r_{\text{glc},R}$  and the regulator becomes a positive feedback loop, to imitate an accelerating establishment of the enzyme pool for glycolysis. A negative feedback of  $\mu$  is introduced in the regulator model because the enzyme pool may be diluted by the cell growth [36]. If  $r_{\text{glc},R} > r_{\text{glc},M}$ , then  $r_{\text{glc}} = r_{\text{glc},M}$  and the regulator will work in a servo mode to follow up  $r_{\text{glc},M}$ . The low pass switch presented by  $K$  in Eq. (29) determines whether the regulated pathway has to be induced or not. Fig. 3 shows the transients of  $r_{\text{glc}}$  (○), the output of the regulator ( $r_{\text{glc},R}$ , –) and the output of the Monod model ( $r_{\text{glc},M}$ , - - -) for experiments.

Mathematically, the regulator model is described by Eqs. (28) and (29).

$$\frac{dr_{\text{glc},R}}{dt} = k_1(r_{\text{glc}} + r_{\text{glc},\text{min}}) + (-k_2 - \mu)r_{\text{glc},R} \quad (28)$$

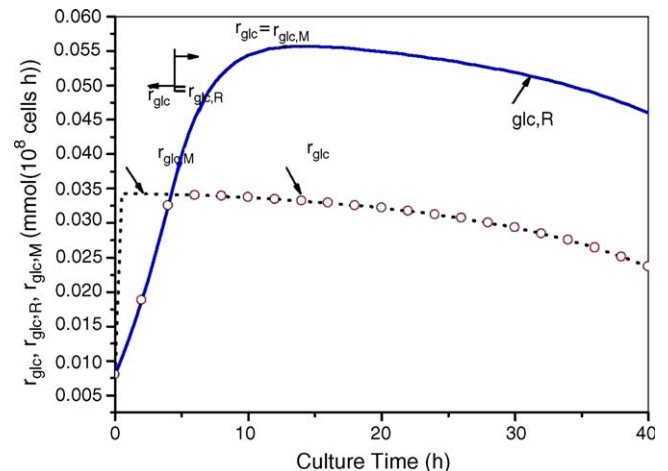


Fig. 3. The specific glucose uptake rate obtained from the modified Monod mode (- - -), the regulator model (-) and output to the macrokinetic model (○).

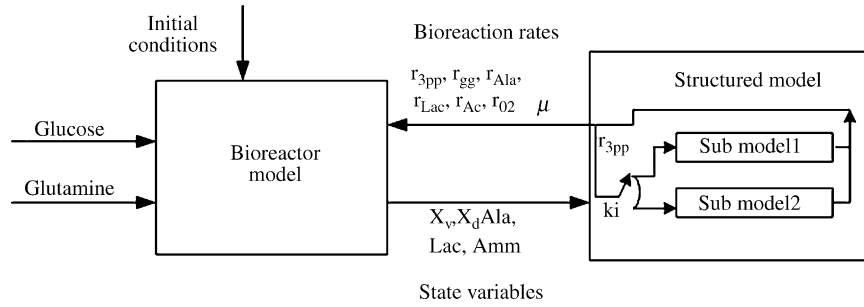


Fig. 4. Combined macrokinetic and bioreactor model.  $K_L$  is the switch, which controls the shift of different modes.

$$r_{glc} = \min\{r_{glc,M}, r_{glc,R}\} \tag{29}$$

The specific glutamine uptake rate is described with a modified Monod kinetic, see Eq. (30) where glutamine [34], ammonia [37,38] and cell density [5,35] are taken into account.

$$r_{gln,M} = r_{gln,max} \frac{S_{gln}}{K_{gln} + S_{gln}} \frac{k_{NH_3gln}}{k_{NH_3gln} + S_{NH_3}} \frac{k_{cgln}}{X_v + k_{cgln}} \tag{30}$$

The mechanisms that lead to cell death are very complex. Apoptosis and necrosis are two general ways of cell death. The exhaustion of limited nutrients was considered as a main reason of cell death [7,39,40]. According to the literature [9,41], the specific death rate is modeled as

$$\mu_d = \mu_{d,max} \left( \frac{k_d}{\mu + k_d} \right)^2 \tag{31}$$

where  $\mu_{d,max}$  is the maximum specific death rate and  $k_d$  is a model parameter.

### 4.3. Bioreactor model

The bioreactor model is obtained by mass balance.

$$\frac{dX_v}{dt} = X_v \frac{\mu - \mu_d - (F_i - R(\cdot))F_o}{V}, \tag{32}$$

$$\text{with } R(\cdot) = \begin{cases} 1 & \text{sampling} \\ 0 & \text{removing supernatant} \end{cases}$$

$$\frac{dX_d}{dt} = X_v \mu_d - X_d \frac{F_i - R(\cdot)F_o}{V} \tag{33}$$

$$X_t = X_v + X_d \tag{34}$$

Table 1  
Identified model parameters in Exps. 1 and 2

$r_{glc,min}$	0.010
$r_{glc,max}$	0.0558
$r_{3pp,min}$	0.0065
$K_{glc}$	0.0002
$k_{cglc}$	10.21
$k_a$	1.796
$k_m$	2.7922
$k_g$	1.2007
$K_{B1}$	0.0231
$K_{B2}$	0.1538
$K_{B3}$	0.0154
$K_{B4}$	0.0251
P/O	2.5
$k_{NH_3gln}$	0.8
$K_{glinglc}$	0.4553
$r_{glnmax}$	0.0303
$m_{ATP}$	0.0001
$K_{gln}$	0.152
$k_{cgln}$	12.41
$\alpha$	0.0050
$\beta$	0.9799
$\tau$	0.0014
$k_1$	0.6319
$k_2$	0.7983
$\mu_{d,max}$	0.0151
$k_d$	0.0081
$Y_{ATP}$	0.16

Units are referred to the Nomenclature.

$$\frac{dGlc}{dt} = -r_{glc}X_v + \frac{Glc_F F_i}{V} - \frac{Glc F_o}{V} \tag{35}$$

$$\frac{dGln}{dt} = -r_{gln}X_v + \frac{Gln_F F_i}{V} - \frac{Gln F_o}{V} \tag{36}$$

Table 2  
The relative change of SSE caused by parameter perturbation around its mean

Parameters	$r_{glnmax}$	$k_{NH_3gln}$	$k_a$	$k_g$	$k_m$	$k_1$	$k_2$	$k_d$	$\mu_{d,max}$
Relative change of $SSE_v$ (%)									
+10% perturbation	24.8	6.1	-8.1	12.4	12.8	6.3	-6.8	0.3	1
-10% perturbation	-17.2	-5.6	12.9	-9.6	-10.5	-8.5	6.3	-0.3	-0.9
Relative change of $SSE_d$ (%)									
+10% perturbation	-13	-5.1	3.1	-4.8	-4.7	-1.3	3.0	-5.9	-4.2
	7.4	3.8	-4.9	4.2	4.3	3.9	-1.3	6.1	5.1

Units are referred to the Nomenclature.

Table 3  
Batch-dependent parameters for Exps. 1–4

Exp. no.	$r_{\text{glnmax}}$	$k_{\text{NH}_3\text{gln}}$	$k_a$	$k_g$	$k_m$	$k_1$	$k_2$	$k_d$	$\mu_{d,\text{max}}$
1 and 2	0.00302	0.8	1.796	1.201	2.792	0.632	0.798	0.008	0.015
3	0.0412	0.6	1.912	1.34	2.782	0.651	0.801	0.0078	0.016
4	0.0323	0.81	1.957	1.38	2.724	0.685	0.793	0.0082	0.012

Units are referred to the Nomenclature.

$$\frac{d\text{Ala}}{dt} = r_{\text{Ala}}X_v - \frac{\text{Ala} F_i}{V} \quad (37)$$

$$\frac{d\text{Lac}}{dt} = r_{\text{Lac}}X_v - \frac{\text{Lac} F_i}{V} \quad (38)$$

$$\frac{d\text{Amm}}{dt} = r_{\text{Amm}}X_v - \frac{\text{Amm} F_i}{V}, \quad \text{with } r_{\text{Amm}} = (1 + \tau)r_{\text{gg}} \quad (39)$$

$$\frac{dV}{dt} = F_i - F_o \quad (40)$$

The coupling of the macrokinetic model and the bioreactor model is depicted in Fig. 4.

### 5. Results and discussion

Batch and fed-batch culture experiments are used to validate the model. In Eqs. (25) and (26), the substrate uptake rates,  $r_{\text{gln}}$  and  $r_{\text{glc}}$ , are modeled with Eqs. (27)–(30). ATP-turnover for maintenance,  $m_{\text{ATP}}$  and the parameters in coefficient matrices can be obtained by parameter identification. After that, the unknown reaction rates,  $r_{\text{gg}}$ ,  $r_{\text{ala}}$ ,  $r_{\text{3pp}}$ ,  $\mu$ ,  $r_{\text{Ac}}$ ,  $r_{\text{O}_2}$ , and  $r_{\text{lac}}$ , may be solved.

In Eqs. (25)–(28) and (30), (31), there are 27 parameters in total. Parameter identification is firstly carried out by try and error. The objective is to minimize the sum of square errors between measured and simulated concentrations of glucose, glutamine and lactate and viable and dead cell densities. The identification results obtained from Exps. 1 and 2 are shown in Table 1.

The sensitivity analysis of the model parameters is carried out by using the method of Claes and Van Impe [42] and the data of Exp. 1. The objective function is the sum of square error presented as Eqs. (41) and (42), where the subscripts v and d represent viable and dead cells, while the superscript S and M denote simulated and measured values, respectively. Perturbation of each parameter by  $\pm 10\%$  around the value listed in Table 1 is applied and the relative change of SSE is calculated. If the relative change of SSE caused by the perturbation exceeds  $\pm 5\%$ , the corresponding parameter is regarded as sensitive one. It is found that 9 out of 27 parameters are sensitive to the perturbations, see Table 2. These nine parameters are further identified with the Simplex method [43] for all experiments while the other parameters take the value in Table 1. The identification results are listed in Table 3.

$$\text{SSE}_v = \sum_{i=1}^{12} \left[ \frac{X_v^S(t) - X_v^M(t)}{X_v^M(t)} \right]^2 \quad (41)$$

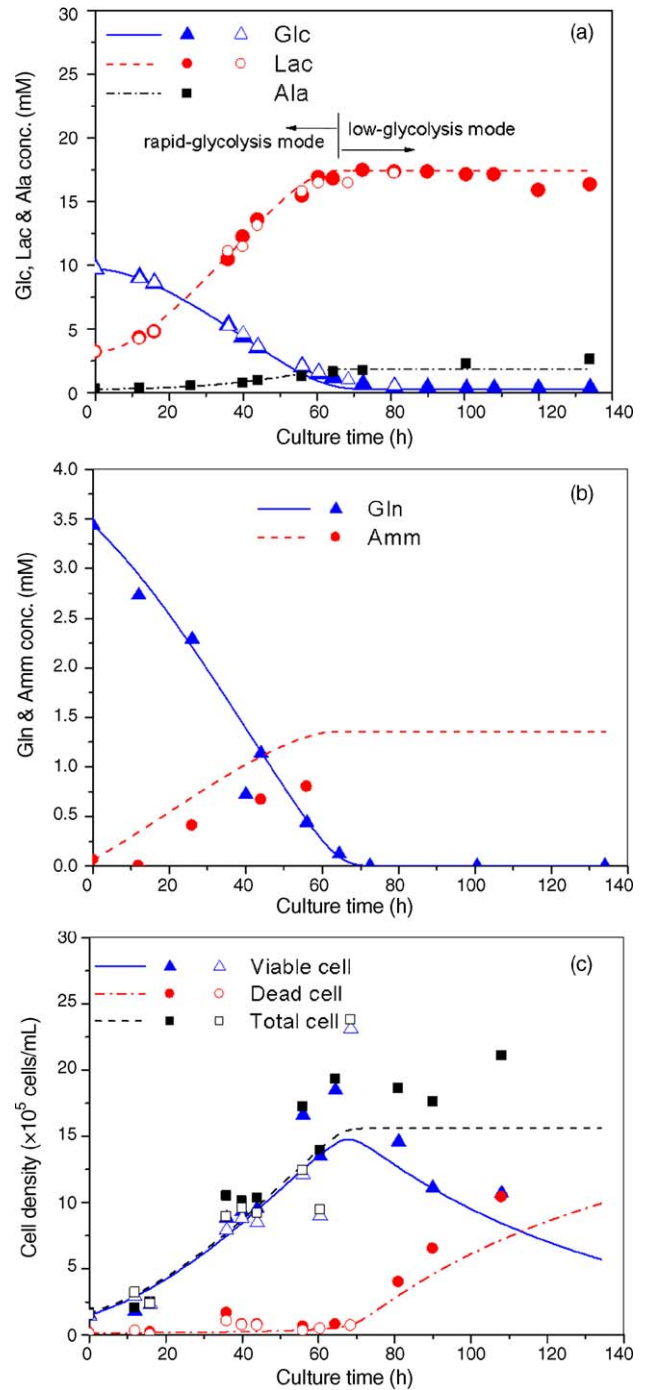


Fig. 5. Comparison between model simulation and measurements after adaptive model parameter identification of Exps. 1 and 2. Lines: model simulations; solid symbols: measurements of Exp. 1; open symbols: measurements of Exp. 2. (a) Concentrations of glucose (Glc), lactate (Lac) and alanine (Ala); (b) concentrations of glutamine (Gln) and ammonia (Amm); (c) densities of viable cell, dead cell and total cell.

$$SSE_d = \sum_{i=1}^{12} \left[ \frac{X_d^S(t) - X_d^M(t)}{X_d^M(t)} \right]^2 \quad (42)$$

where  $i$  is the sampling number of Exp. 1.

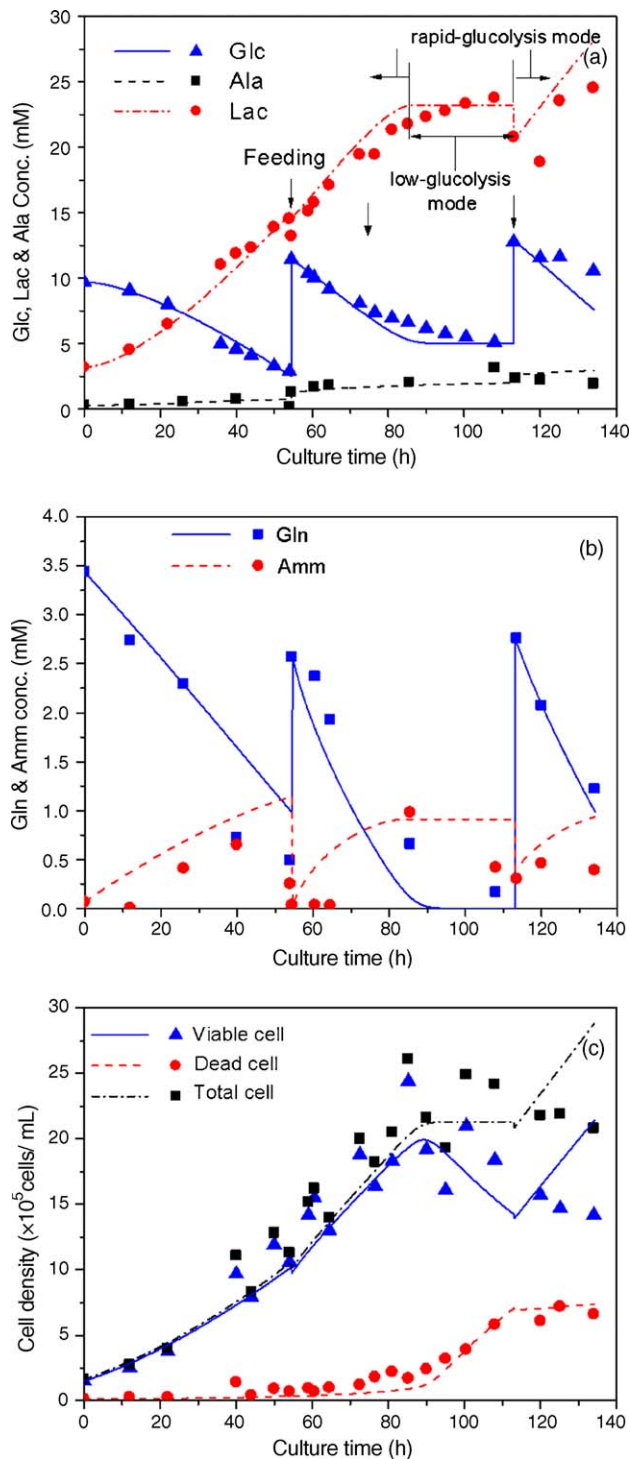


Fig. 6. Comparison between model simulation and measurements after adaptive model parameter identification of Exp. 3. Lines: model simulations; solid symbols: measurements. (a) Concentrations of glucose (Glc), lactate (Lac) and alanine (Ala); (b) concentrations of glutamine (Gln) and ammonia (Amm); (c) densities of viable cell, dead cell and total cell.

After parameter identification, comparison between model simulations and measurements are shown in Figs. 5–7. Qualitatively, the profiles of glucose, lactate, glutamine, alanine, ammonia, viable cell density, dead cell density and total cell density are well simulated by the model. Metabolic

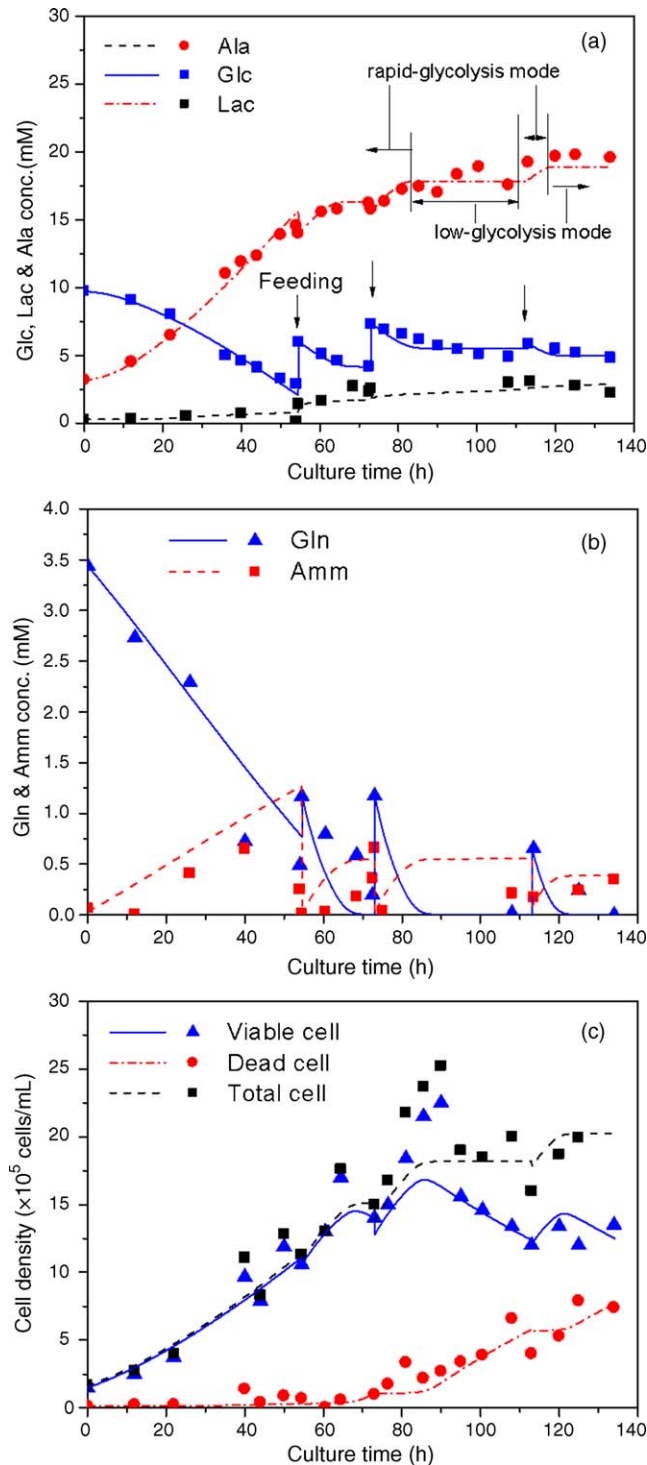


Fig. 7. Comparison between model simulation and measurements after adaptive model parameter identification of Exp. 4. Lines: model simulations; solid symbols: measurement. (a) Concentrations of glucose (Glc), lactate (Lac) and alanine (Ala); (b) concentrations of glutamine (Gln) and ammonia (Amm); (c) densities of viable cell, dead cell and total cell.

shifts are found in Exps. 1, 3 and 4. In Exp. 1, metabolic shift happens at 79 h (see Fig. 1(a)), where the model switches from rapid-glycolysis mode to low-glycolysis mode, and lactate production ceases. There are two times of metabolic shifts in Exp. 3. The first one happens at 105 h (see Fig. 6(a)), where the model switches from rapid-glycolysis mode to low-glycolysis mode. The second one happens at 113 h, where the model switches from low-glycolysis mode to rapid-glycolysis mode again. In Exp. 4, three metabolic shifts happened at 90, 113 and 125 h, respectively, see Fig. 7(a).

Regulator model for specific glucose uptake rate works well in these experiments. At the beginning of the experiments and the period after feeding, regulator model for specific glucose uptake rate operates. In Exps. 1 and 2, regulator model keeps on working until 12.8 h, when the specific glucose uptake rate is low, and the glucose concentration is high. After that, model switches to Monod one. In Exp. 3, regulator model operates twice. The first one works from the beginning of the experiment to 9.9 h, and the second one operates from 113 to 114.7 h. In Exp. 4, regulator model operates during the following periods, 0–11, 73.1–74.4 and 113–114.1 h, respectively.

$Y_{\text{ATP}}$  and  $P/O$  are taken as fixed values in the paper. But in growing microorganisms,  $Y_{\text{ATP}}$  depends markedly on the growth rate and on environmental parameters such as the different carbon sources, pH, temperature, and the ionic strength of the medium. [44].  $P/O$  changes depending on the growth phases or flux rates of keynote metabolites [45,46]. Principally, a variation of  $P/O$  may be taken into account in the modeling after the relationship between  $P/O$  and its influencing factors becomes clear.

## 6. Conclusion

Based on the analysis of metabolic pathways of myeloma cell line, a macrokinetic model is established. The model delivers the simulation of key bioreaction rates, such as  $r_{\text{gg}}$ ,  $r_{\text{ala}}$ ,  $r_{\text{3pp}}$ ,  $\mu$ ,  $r_{\text{Ac}}$ ,  $r_{\text{O}_2}$ , and  $r_{\text{lac}}$ . The macrokinetic model is further combined with bioreactor model so that the state variables, such as concentrations of glucose, glutamine, alanine and ammonia, viable cell density, death cell density and total cell density, are predicted. Simulation results demonstrate that the experimental data of cell growth and cell death, uptake of glucose and glutamine, and production of lactate in both batch and fed-batch cultures can be described by the combined macrokinetic and bioreactor model with reasonable accuracy. Relatively small deviation of the identified sensitive parameters among different experiments indicates the robustness of the model. These results may lead to the conclusion that the simplified structure of the metabolic network on which the model is based covers the major features of the cell line concerned.

However, some limitations still exist in the model. For example, the specific glucose uptake rate is well described by the regulator model (combined with Monod kinetics), the biological mechanism of regulator model needs to be explained. In addition, the balance for oxygen consumption and carbon dioxide production as well as the balance of NADPH are not taken into account in the model due to the lack

of data, which is also a shortage of the present work, and needs further investigations.

## Acknowledgements

The authors gratefully acknowledge the financial support of the Natural Science Foundation of China (grant no. 60574038 and 20576136), the German DAAD Postdoc Scholarship, and the DFG/Germany-MOE/China Exchange Program.

## Appendix A. Nomenclature

Ala	alanine concentration in medium (mM)
Amm	ammonia concentration in medium (mM)
$F_i$	input flow rate ( $\text{L h}^{-1}$ )
$F_o$	output flow rate ( $\text{L h}^{-1}$ )
Glc	glucose concentration in medium (mM)
Gln	glutamine concentration in medium (mM)
$k_1, k_2, k'_1, k'_2, k_a, k_g, k_m, k_{\text{dglN}}, k_{\text{cglc}}, k_{\text{cglN}}, k_d, k_{\text{NH}_3\text{gln}}, K_{\text{gln}}, K_{\text{glc}}, K_{\text{gInglc}}, K_{\text{B1}}, K_{\text{B2}}, K_{\text{B3}}, K_{\text{B4}}$	model parameters
Lac	lactate concentration in medium (mM)
$m_{\text{ATP}}$	maintenance coefficient for ATP ( $\text{mmol} (\times 10^8 \text{ cells h})^{-1}$ )
$M$	metabolite concentration in medium (mM)
$P/O$	effectiveness coefficient of oxidative phosphorylation
$r_{\text{Ac}}$	specific acetyl CoA production rate ( $\text{mmol} (\times 10^8 \text{ cells h})^{-1}$ )
$r_{\text{ala}}$	specific alanine production rate ( $\text{mmol} (\times 10^8 \text{ cells h})^{-1}$ )
$r_{\text{ATP}}$	specific ATP uptake rate ( $\text{mmol} (\times 10^8 \text{ cells h})^{-1}$ )
$r_{\text{B1}}, r_{\text{B2}}, r_{\text{B3}}, r_{\text{B4}}$	specific bio-synthesis rate of biomass ( $\text{mmol} (\times 10^8 \text{ cells})^{-1}$ )
$r_{\text{ck}}$	specific $\alpha$ -kg production rate from $\alpha$ -kg in TCA cycle ( $\text{mmol} (\times 10^8 \text{ cells h})^{-1}$ )
$r_{\text{gg}}$	specific glutaminolysis rate ( $\text{mmol} (\times 10^8 \text{ cells h})^{-1}$ )
$r_{\text{glc}}$	specific glucose uptake rate in the macrokinetic model ( $\text{mmol} (\times 10^8 \text{ cells h})^{-1}$ )
$r_{\text{glc,M}}$	specific glucose uptake rate obtained from Monod model ( $\text{mmol} (\times 10^8 \text{ cells h})^{-1}$ )
$r_{\text{glc,R}}$	specific glucose uptake rate obtained from regulator model ( $\text{mmol} (\times 10^8 \text{ cells h})^{-1}$ )
$r_{\text{gln}}$	specific glutamine uptake rate in the macrokinetic model ( $\text{mmol} (\times 10^8 \text{ cells h})^{-1}$ )
$r_{\text{gln,M}}$	specific glutamine uptake rate obtained from Monod model ( $\text{mmol} (\times 10^8 \text{ cells h})^{-1}$ )

$r_{\text{glN,R}}$	specific glutamine uptake rate obtained from regulator model ( $\text{mmol} (\times 10^8 \text{ cells h}^{-1})$ )
$r_{\text{G6P}}$	specific glycolysis rate ( $\text{mmol} (\times 10^8 \text{ cells h}^{-1})$ )
$r_{\text{km}}$	specific malate production rate from citrate in TCA cycle ( $\text{mmol} (\times 10^8 \text{ cells h}^{-1})$ )
$r_{\text{Lac}}$	specific lactate production rate ( $\text{mmol} (\times 10^8 \text{ cells h}^{-1})$ )
$r_{\text{mm}}$	specific pyruvate production rate from malate coming from mitochondrion ( $\text{mmol} (\times 10^8 \text{ cells h}^{-1})$ )
$r_{\text{NADH}}$	specific NADH uptake rate in respiratory chain ( $\text{mmol} (\times 10^8 \text{ cells h}^{-1})$ )
$r_{\text{O}_2}$	specific oxygen uptake rate ( $\text{mmol} (\times 10^8 \text{ cells h}^{-1})$ )
$r_{\text{TCC}}$	specific acetyl CoA uptake rate ( $\text{mmol} (\times 10^8 \text{ cells h}^{-1})$ )
$r_{\text{3pp}}$	specific 3-phosphoglycerate production rate ( $\text{mmol} (\times 10^8 \text{ cells h}^{-1})$ )
$r_{\text{3pp,min}}$	threshold value of generating lactate ( $\text{mmol} (\times 10^8 \text{ cells h}^{-1})$ )
$V$	culture volume (L)
$X_{\text{d}}$	dead cell density ( $\times 10^5 \text{ cells mL}^{-1}$ )
$X_{\text{t}}$	total cell density ( $\times 10^5 \text{ cells mL}^{-1}$ )
$X_{\text{v}}$	viable cell density ( $\times 10^5 \text{ cells mL}^{-1}$ )
$Y_{\text{ATP}}$	yield coefficient of ATP ( $\times 10^8 \text{ cells} (\text{mmol ATP})^{-1}$ )

#### Greek letters

$\alpha$	the fraction of 3P synthesizing serine
$\beta$	the fraction of pyruvate oxidized to lactate
$\mu$	specific growth rate ( $\text{h}^{-1}$ )
$\mu_{\text{d,max}}$	the maximum specific death rate ( $\text{h}^{-1}$ )
$\tau$	the fraction of glutamate converted to $\alpha$ -ketoglutarate

#### References

- Miller WM, Blanch HW, Wilke CR. A kinetic analysis of hybridoma growth and metabolism in batch and continuous suspension culture: effect of nutrient concentration, dilution rate, and pH. *Biotechnol Bioeng* 1988;32:947–65.
- Miller WM, Blanch HW. Regulation of animal cell metabolism in bioreactors. In: Ho CS, Wang DIC, editors. *Animals Cells Bioreactors*. Stoneham, MA: Butterworth-Heinemann; 1991. p. 119–61.
- Zupke C, Sinskey AJ, Stephanopoulos G. Intracellular flux analysis applied to the effect of dissolved oxygen on hybridoma. *Appl Microb Biotechnol* 1995;44:27–36.
- Ljunggren J, Haggstrom L. Specific growth rate as a parameter for tracing growth-limiting substances in animal cultures. *J Biotechnol* 1995;42:163–75.
- Zeng A-P. Quantitative assessment of cell density effect on the metabolism and antibody production rate of hybridoma cells at high cell density. *J Biotechnol* 1996;45:243–51.
- Zeng A-P, Deckwer W-D, Hu W-S. Determinant and rate laws of growth and death of hybridoma cells in continuous culture. *Biotechnol Bioeng* 1998;57:642–54.
- Portner R, Schafer T. Modeling hybridoma cell growth and metabolism—a comparison of selected models and data. *J Biotechnol* 1996;49:119–35.
- Bibila T, Flickinger MC. A structured model for monoclonal antibody synthesis in exponentially growing and stationary phase hybridoma cells. *Biotechnol Bioeng* 1991;37:210–26.
- Sanderson CS, Barford JP, Barton GW. A structured, dynamic model for animal cell culture system. *Biochem Eng J* 1999;3:203–11.
- Sanderson CS, Barford JP, Barton GW. A structured, dynamic model for animal cell culture system: application to murine hybridoma. *Biochem Eng J* 1999;3:213–8.
- Sanderson CS, Barford JP, Barton GW. A structured, dynamic model for animal cell culture: application to baculovirus/insect cell system. *Biochem Eng J* 1999;3:219–29.
- Namjoshi AA, Hu W-S, Ramkrishna D. Unveiling steady-state multiplicity in hybridoma cultures: the cybernetic approach. *Biotechnol Bioeng* 2003;81:80–91.
- K.H. Bellgardt, Modellbildung des wachstums von *Saccharomyces cerevisiae* in rührkesselreaktoren. PhD thesis, University of Hannover, 1983.
- Pham HTB, Larsson G, Enfors S-O. Growth and energy metabolism in aerobic fed-batch cultures of *Saccharomyces cerevisiae* simulation and model verification. *Biotechnol Bioeng* 1998;60:474–82.
- Ren HT, Yuan JQ, Bellgardt KH. Macrokinetic model for methylotrophic *Pichia pastoris* based on stoichiometric balance. *J Biotechnol* 2003;106(1):53–68.
- Xie LZ, Wang DIC. Material balance studies on animal cell metabolism using a stoichiometrically based reaction network. *Biotechnol Bioeng* 1996;52:579–90.
- Xie LZ, Wang DIC. Energy metabolism and ATP balance in animal cell cultivation using a stoichiometrically based reaction network. *Biotechnol Bioeng* 1996;52:591–601.
- Bonarius HPJ, Hatzimanikatis V, Meesters KPH, de Gooijer CD, Schmid G, Tramper J. Metabolic flux analysis of hybridoma cells in different culture media using mass balances. *Biotechnol Bioeng* 1996;50:299–318.
- Bonarius HPJ, Ozemre A, Timmerarends B, Skrabal P, Tramper J, Schmid G, Heinzle E. Metabolic-flux analysis of continuously cultured hybridoma cells using  $^{13}\text{C}$  mass spectrometry in combination with  $^{13}\text{C}$ -lactate nuclear magnetic resonance spectroscopy and metabolite balancing. *Biotechnol Bioeng* 2001;74:529–38.
- Korke R, de Leon GM, Lau A, Lei Y, Lim JWE, Seow TK, Chung MCM, Hu W-S. Large scale gene expression profiling of metabolic shift of mammalian cells in culture. *J Biotechnol* 2004;107:1–17.
- Sanfeliu A, Paredes C, Cairo JJ, Godia F. Identification of key patterns in the metabolism of hybridoma cells in culture. *Enzyme Microb Technol* 1997;21:421–8.
- Zhou W, Rehm J, Europa A, Hu W-S. Alteration of mammalian cell metabolism by dynamic nutrient feeding. *Cytotechnology* 1997;14:99–108.
- Follstad BD, Balcarel RR, Stephanopoulos G, Wang DIC. Metabolic flux analysis of hybridoma continuous culture steady state multiplicity. *Biotechnol Bioeng* 1999;63:675–83.
- Europa AF, Gambhir A, Fu P-C, Hu W-S. Multiple steady states with distinct cellular metabolism in continuous culture of mammalian cells. *Biotechnol Bioeng* 2000;67:25–34.
- Zhou W, Chen CC, Buckland B, Aumins J. Fed-batch culture of recombinant NS0 myeloma cells with high monoclonal antibody production. *Biotechnol Bioeng* 1997;55:783–92.
- Xie LZ, Wang DIC. Stoichiometric analysis of animal cell growth and its application in medium design. *Biotechnol Bioeng* 1994;43:1164–74.
- Zupke C, Stephanopoulos G. Intracellular flux analysis in hybridoma using mass balances and in vitro  $^{13}\text{C}$  NMR. *Biotechnol Bioeng* 1995;45:292–303.
- Zupke C. Metabolic flux analysis in mammalian cell culture. PhD thesis, Massachusetts Institute of Technology, 1993.
- Paredes C, Sanfeliu A, Cairo JJ, Godia F. Estimation of the intracellular fluxes for a hybridoma cell line by material balances. *Enzyme Microb Technol* 1998;23:187–98.
- Pirt SJ. The maintenance energy of bacteria in growing culture. *Proc R Soc Lond Ser B: Biol Sci* 1965;163:224–31.

- [31] Dalili M, Sayles GD, Ollis DF. Glutamine-limited batch hybridoma growth and antibody production: experiment and model. *Biotechnol Bioeng* 1990;36:74–82.
- [32] Lei F, Rotboll M, Jorgensen SB. A biochemically structured model for *Saccharomyces cerevisiae*. *J Biotechnol* 2001;88:205–21.
- [33] Provost A, Bastin G. Dynamic metabolic modeling under the balanced growth condition. *J Proc Cont* 2004;14:717–28.
- [34] Jeong Y-H, Wang SS. Role of glutamine in hybridoma cell culture: effects on cell growth, antibody production, and cell metabolism. *Enzyme Microb Technol* 1995;17:47–55.
- [35] Banik GG, Heath CA. Hybridoma growth and antibody production as a function of cell density and specific growth rate in perfusion culture. *Biotechnol Bioeng* 1995;48:289–300.
- [36] Bellgardt KH, Meyer HD, Kuhlmann W, Schuegerl K, Thoma M. Application of an extended Kalman filter for state estimation for state estimation of a yeast fermentation. *IEEE Proc* 1986;133:226–41.
- [37] Schneider M, Alaoui MEI, von Stokar U, Marison IW. Batch cultures of a hybridoma cell line performed with in situ ammonia removal. *Enzyme Microb Technol* 1997;20:268–76.
- [38] Bonarius HPJ, Houtman JHM, de Gooijer CD, Tramper J, Schmid G. Activity of glutamate dehydrogenase is increased in ammonia-stressed hybridoma cells. *Biotechnol Bioeng* 1998;57:447–53.
- [39] Simpson NH, Singh RP, Perani A, Goldenzon C, Rubeai MA. In hybridoma cultures, deprivation of any single amino acid leads to apoptotic death, which is suppressed by the expression of the bcl-2 gene. *Biotechnol Bioeng* 1998;59:90–8.
- [40] Tinto A, Gabernet C, Vives J, Prats E, Cairo JJ, Cornudella L, Godia F. The protection of hybridoma cells from apoptosis by caspase inhibition allows culture recovery when exposed to non-inducing conditions. *J Biotechnol* 2002;95:205–14.
- [41] Zeng A-P, Bi J. Cell culture kinetics and modeling. In: Ozturk SS, Hu W-S, editors. *Cell Culture Technology for Pharmaceutical and Cellular Therapies*. Atlanta: Taylor and Francis Group; 2005. p. 299–347.
- [42] Claes JE, Van Impe JE. Combining yield coefficients and exit-gas analysis for monitoring of the baker's yeast fed-batch fermentation. *Bioproc Eng* 2000;22:195–200.
- [43] Nelder R, Mead JA. A simplex method for function minimization. *Comput J* 1965;7:308–13.
- [44] Zeng AP, Ross A, Deckwer W-D. A method to estimate the efficiency of oxidative phosphorylation and biomass yield from ATP of a facultative anaerobe in continuous culture. *Biotechnol Bioeng* 1990;36:965–9.
- [45] Fontaine EM, Devin A, Rigoulet M, Leverve XM. The yield of oxidative phosphorylation is controlled both by force and flux. *Biochem Biophys Res Commun* 1997;232:532–5.
- [46] Kadenbach B. Intrinsic and extrinsic uncoupling of oxidative phosphorylation. *Biochim Biophys Acta* 2003;1604:77–94.